universe

MDPI

Article

Effect of Spin-Dependent Short-Range Correlations on Nuclear Matrix Elements for Neutrinoless Double Beta Decay of ^{48}Ca

Shahariar Sarkar [1] and Yoritaka Iwata [2,*]

[1] Department of Physics, Indian Institute of Technology Roorkee, Roorkee 247 667, India; shahariar.ph@sric.iitr.ac.in
[2] Faculty of International Studies, Osaka University of Economics and Law, Yao 581-0853, Japan
* Correspondence: iwata_phys@08.alumni.u-tokyo.ac.jp

Abstract: Neutrinoless double beta decay is a pivotal weak nuclear process that holds the potential to unveil the Majorana nature of neutrinos and predict their absolute masses. In this study, we delve into examining the impact of spin-dependent short-range correlations (SRCs) on the nuclear matrix elements (NMEs) for the light neutrino-exchange mechanism in neutrinoless double beta ($0\nu\beta\beta$) decay of ^{48}Ca, employing an extensive interacting nuclear shell model. All computations are performed employing the effective shell model Hamiltonian GXPF1A, encompassing the entire fp model space through the closure approximation. Our investigation examines the NMEs' dependencies on factors such as the number of intermediate states, coupled spin-parity attributes of neutrons and protons, neutrino momentum, inter-nucleon separation, and closure energy. This scrutiny is performed with respect to both the conventional Jastrow-type approach of SRCs, employing various parameterizations, and the spin-dependent SRC paradigm. Our findings illuminate a discernible distinction in NMEs induced by spin-dependent SRCs, differing by approximately 10–20% from those computed through the conventional Jastrow-type SRCs, incorporating distinct parameterizations.

Keywords: neutrinoless double beta decay; short-range correlations; nuclear shell model

Citation: Sarkar, S.; Iwata, Y. Effect of Spin-Dependent Short-Range Correlations on Nuclear Matrix Elements for Neutrinoless Double Beta Decay of ^{48}Ca. *Universe* **2023**, *9*, 444. https://doi.org/10.3390/universe9100444

Academic Editors: Mihai Horoi, Hiro Ejiri and Andrei Neacsu

Received: 16 August 2023;
Revised: 23 September 2023
Accepted: 27 September 2023
Published: 3 October 2023

1. Introduction

Neutrinoless double beta decay ($0\nu\beta\beta$) is a rare and crucial weak nuclear decay that occurs in certain even–even nuclei such as ^{48}Ca, ^{76}Ge, ^{82}Se, ^{96}Zr, ^{100}Mo, ^{116}Cd, ^{124}Sn, ^{130}Te, ^{126}Xe, etc. In this process, two neutrons inside the decaying nucleus are converted into two protons and two electrons without emitting any neutrinos that violate the lepton number conservation. The neutrino appears as a virtual intermediate Majorana particle [1–5]. Although predicted long back in 1939 by Wolfgang Furry [6,7] based on E. Majorana's symmetric theory for fermion and anti-fermion [8] followed by G. Racah's chain reactions [9] in 1937, this rare process has yet to be observed by experiment. However, observing this rare process would prove the existence of the Majorana neutrino, which is indeed widely favored in many beyond the standard model (BSM) physics theories for the explanation of the smallness of neutrino mass [10–12]. Furthermore, there is no definite value of absolute neutrino mass measured yet by experiment. An upper limit for the absolute neutrino mass of 0.8 eV has been derived through the tritium beta decay experiment-KATRIN [13] and the precise upper limit on the effective Majorana neutrino mass of 36–156 meV is predicted in $0\nu\beta\beta$ decay experiment KamLAND-Zen on ^{136}Xe [14]. In this context, the $0\nu\beta\beta$ process can also provide information on the absolute mass scale of neutrinos [5,15], which makes this process more interesting.

A number of particle physics mechanisms have been proposed for the $0\nu\beta\beta$ decay process. One of them is the widely studied standard light neutrino-exchange mechanism [16,17], which will also be the focus of this study. Other mechanisms include the heavy neutrino-exchange mechanism [7], the left-right symmetric mechanisms [18,19], the supersymmetric particle exchange mechanisms [20,21], etc.

The half-life for $0\nu\beta\beta$ decay is connected with absolute neutrino mass through a quantity called the nuclear matrix elements (NMEs), which are theoretically calculated in different nuclear many-body models [4] such as quasiparticle random phase approximation (QRPA) [7], the interacting shell-model (ISM) [22–26], the interacting boson model (IBM) [27,28], the generator coordinate method (GCM) [29–31], energy density functional (EDF) theory [29,30], relativistic energy density functional (REDF) theory [30,31], and the projected Hartree–Fock–Bogolibov model (PHFB) [32], the ab initio variational Monte Carlo (VMC) technique [33–35], etc. The accuracy of NME calculations plays an important role in predicting the correct value for the half-life of $0\nu\beta\beta$ decay and absolute neutrino mass. Hence, calculating the NMEs accurately is one of the central themes of research for studying the $0\nu\beta\beta$ decay.

Around the world, several major experimental investigations are being carried out for different $0\nu\beta\beta$ decaying candidates such as GERDA (^{76}Ge), MAJORANA DEMONSTRATOR (^{76}Ge), LEGEND (^{76}Ge), CUORE (^{130}Te), CUPID (^{82}Se/^{100}Mo/^{130}Te), AMoRE (^{100}Mo), EXO-200 (^{136}Xe), nEXO (^{136}Xe), NEXT (^{136}Xe), PandaX-III (^{136}Xe), KamLAND-Zen and KamLAND2-Zen (^{136}Xe), CANDLES (^{48}Ca), and Super-NEMO (^{82}Se) [1]. Our particular interest in this study is the $0\nu\beta\beta$ decay of ^{48}Ca, which is one of the simplest decay candidates with significant experimental interest. In particular, we aim to examine the effect of spin-dependent SRCs on the NMEs for the $0\nu\beta\beta$ decay of ^{48}Ca using the nuclear shell model.

$0\nu\beta\beta$ decay in ^{48}Ca proceeds as:

$$^{48}\mathrm{Ca} \rightarrow ^{48}\mathrm{Ti} + e^- + e^-. \tag{1}$$

The computation of NMEs corresponding to the light neutrino-exchange mechanism of the $0\nu\beta\beta$ decay in ^{48}Ca was carried out in several studies ([23–25,36–42]). In these investigations, the influences of SRCs were integrated through a Jastrow-type approach [43,44], characterizing the radial-dependence effects of SRCs. An alternative method, known as the Unitary Correlation Operator Method (UCOM) [45–47], also accounted for SRCs via radial dependence. More recently, in a notable advancement [48], the interplay of spin in conjunction with SRCs was incorporated to compute NMEs for the light neutrino-exchange $0\nu\beta\beta$ decay in ^{48}Ca. This study, however, operated within a confined valence space, focusing exclusively on the $f_{7/2}$ orbital within the pf-shell. The main findings in Ref. [48] emphasize that accounting for spin-dependent SRCs leads to an approximate 20% reduction in the NMEs when compared to the no-SRC scenario within the pure shell model framework.

Motivated by these advances, our current endeavor aims to expand the computational scope. Specifically, we engage the complete fp model space encompassing the orbitals $0f_{7/2}$, $0f_{5/2}$, $1p_{3/2}$, and $1p_{1/2}$ for ^{48}Ca. This comprehensive approach enables us to thoroughly assess the cumulative effect of spin on SRCs for the $0\nu\beta\beta$ decay in ^{48}Ca. Furthermore, we undertake an in-depth exploration of the variances between the spin-dependent SRC scenario and the conventional Jastrow-type SRC approach. We systematically investigate the dependencies of NMEs on factors such as the coupled spin-parity of protons and neutrons, the number of intermediate states, neutrino momentum, inter-nucleon separation, and closure energy. Our goal is to uncover how these dependencies diverge under the influence of spin-dependent SRCs and to contrast them with the outcomes of the traditional Jastrow-type SRC approach. As our investigation progresses, we envision extending this approach to encompass other decay candidates within the $0\nu\beta\beta$ realm, thereby offering a more comprehensive understanding of this intriguing nuclear process.

Driven by this motivation, the rest of this paper is structured as follows. Section 2 outlines the formulation of the decay rate, NMEs, and transition operators pertinent to $0\nu\beta\beta$ decay. In Section 3, we delve into the integration of SRC effects within both the Jastrow-type approach and the spin-dependent approach. The methodology for calculating NMEs using the shell model within the closure method is detailed in Section 4. Subsequently, Section 5 presents the comprehensive results and initiates discussions around the observed outcomes. Lastly, Section 6 encapsulates the synthesis of our findings and delineates potential avenues for future exploration.

2. The Decay Rate and NMEs for $0\nu\beta\beta$ Decay

The decay rate for the light neutrino-exchange mechanism of $0\nu\beta\beta$ decay can be written as [17]

$$[T^{0\nu}_{\frac{1}{2}}]^{-1} = G^{0\nu}|M^{0\nu}|^2\left(\frac{\langle m_{\beta\beta}\rangle}{m_e}\right)^2, \tag{2}$$

where $G^{0\nu}$ is the phase-space factor that can be calculated accurately [49], $M^{0\nu}$ is the total nuclear matrix element for the light neutrino-exchange mechanism, and $m_{\beta\beta}$ is the effective Majorana neutrino mass defined by the neutrino mass eigenvalues m_k and the neutrino mixing matrix elements U_{ek}

$$\langle m_{\beta\beta}\rangle = \left|\sum_k m_k U^2_{ek}\right|. \tag{3}$$

The total nuclear matrix element $M^{0\nu}$ is the sum of Gamow–Teller (M_{GT}), Fermi (M_F), and tensor (M_T) matrix elements, as given by [5]:

$$M^{0\nu} = M_{GT} - \left(\frac{g_V}{g_A}\right)^2 M_F + M_T, \tag{4}$$

where g_V and g_A are the vector and axial-vector constants, respectively. In this study, $g_V = 1$ and the bare value of $g_A = 1.27$ is used. The matrix elements M_{GT}, M_F, and M_T of transition operator O^{α}_{12} of $0\nu\beta\beta$ decay are expressed as [25]:

$$M_\alpha = \langle f|O^{\alpha}_{12}|i\rangle \tag{5}$$

where $\alpha \in F, GT, T$, $|i\rangle$ corresponds to the 0^+ ground state of the parent nucleus ^{48}Ca in the present study, and $|f\rangle$ corresponds to the 0^+ ground state of the granddaughter nucleus ^{48}Ti.

The calculation of two-body matrix elements (TBMEs) for $0\nu\beta\beta$ decay scalar two-particle transition operators O^{α}_{12} have both spin and radial neutrino potential parts. These operators are given by [24]:

$$\begin{aligned} O^{GT}_{12} &= \tau_{1-}\tau_{2-}(\boldsymbol{\sigma_1}\cdot\boldsymbol{\sigma_2})H_{GT}(r,E_k),\\ O^{F}_{12} &= \tau_{1-}\tau_{2-}H_F(r,E_k),\\ O^{T}_{12} &= \tau_{1-}\tau_{2-}S_{12}H_T(r,E_k), \end{aligned} \tag{6}$$

where, τ is the isospin annihilation operator, $\boldsymbol{r} = \boldsymbol{r_1} - \boldsymbol{r_2}$ is the inter-nucleon distance of the decaying nucleons, and $r = |\boldsymbol{r}|$. The operator S_{12} is defined as $S_{12} = 3(\boldsymbol{\sigma_1}\cdot\hat{\boldsymbol{r}})(\boldsymbol{\sigma_2}\cdot\hat{\boldsymbol{r}}) - (\boldsymbol{\sigma_1}\cdot\boldsymbol{\sigma_2})$. For the light neutrino-exchange mechanism of $0\nu\beta\beta$ decay, the radial neutrino potential with explicit dependence on the energy of the intermediate states is given by [24]:

$$H_\alpha(r,E_k) = \frac{2R}{\pi}\int_0^\infty \frac{f_\alpha(q,r)qdq}{q + E_k - (E_i+E_f)/2}, \tag{7}$$

where R is the radius of the parent nucleus, q is the momentum of the virtual Majorana neutrino, E_i, E_k, and E_f are the energies of the initial, intermediate, and final nuclei, $f_\alpha(q,r) = j_p(q,r)h_\alpha(q,r)$ with $j_p(q,r)$ is a spherical Bessel function with $p = 0$ for Fermi and Gamow–Teller type NMEs and $h_\alpha(q,r)$ is the term that accounts for the effects of higher-order currents (HOC) and finite nucleon size (FNS) [17] given by [17,43]:

$$h_F(q^2) = g_V^2(q^2), \tag{8}$$

$$h_{GT}(q^2) = \frac{g_A^2(q^2)}{g_A^2}\left(1 - \frac{2}{3}\frac{q^2}{q^2+m_\pi^2} + \frac{1}{3}\left(\frac{q^2}{q^2+m_\pi^2}\right)^2\right) + \frac{2}{3}\frac{g_M^2(q^2)}{g_A^2}\frac{q^2}{4m_p^2}, \tag{9}$$

$$h_T(q^2) = \frac{g_A(q^2)}{g_A^2}\left(\frac{2}{3}\frac{q^2}{q^2+m_\pi^2} - \frac{1}{3}\left(\frac{q^2}{q^2+m_\pi^2}\right)^2\right) + \frac{1}{3}\frac{g_M^2(q^2)}{g_A^2}\frac{q^2}{4m_p^2}. \tag{10}$$

In this regard, the $g_V(q^2)$, $g_A(q^2)$, and $g_M(q^2)$ form factors, which account for FNS effects, are used. In the dipole approximation, the form factors are given by the following Equations [17,23]:

$$g_V(q^2) = \frac{g_V}{\left(1+\frac{q^2}{M_V^2}\right)^2}, \tag{11}$$

$$g_A(q^2) = \frac{g_A}{\left(1+\frac{q^2}{M_A^2}\right)^2}, \tag{12}$$

$$g_M(q^2) = (\mu_p - \mu_n) g_V(q^2). \tag{13}$$

where g_V, g_A, μ_p, and μ_n are the vector, axial-vector, and magnetic moment coupling constants for the nucleon, and M_V and M_A are the vector and axial-vector meson masses, respectively. The values of M_V and M_A are 850 MeV and 1086 MeV, respectively, while a $\mu_p - \mu_n$ value of 4.7 is used in the calculation [23]. The masses of the proton and pion are denoted by m_p and m_π, respectively.

3. The Effects of Short-Range Correlations on $0\nu\beta\beta$ Decay

In the computation of the NMEs for $0\nu\beta\beta$ decay, it becomes imperative to factor in the influences of SRCs, as discussed previously. Over time, various techniques have been employed to integrate SRC effects into NME calculations for $0\nu\beta\beta$ decay. One of the extensively utilized and classical methodologies is known as the Jastrow approach, as discussed in references [43,44]. More recently, a novel spin-dependent approach has emerged, as outlined in reference [48]. Both of these methodologies are delineated comprehensively below.

3.1. The Jastrow Approach

A standard method to include SRCs is via a phenomenological Jastrow-like function [43,44]. By including the SRC effect in the Jastrow approach, one can write the NMEs of $0\nu\beta\beta$ defined in Equation (5) as [43]

$$M_\alpha = \langle f | f_{Jastrow}(r) O_{12}^\alpha f_{Jastrow}(r) | i \rangle, \tag{14}$$

where the Jastrow-type SRC function is defined as

$$f_{Jastrow}(r) = 1 - ce^{-ar^2}(1 - br^2). \tag{15}$$

In the literature, three different SRC parameterizations are used: Miller–Spencer, Charge-Dependent-Bonn (CD-Bonn), and Argonne V18 (AV18) to parameterize a, b, and c [23]. The parameters a, b, and c in different SRC parameterizations are given in Table 1.

This approach of using a Jastrow-like function to include the effects of SRCs is extensively used in Refs. [23,41,42].

Table 1. Parameters for the Jastrow-type function of Equation (15).

SRC Type	*a*	*b*	*c*
Miller–Spencer	1.10	0.68	1.00
CD-Bonn	1.52	1.88	0.46
AV18	1.59	1.45	0.92

3.2. Spin-Dependent Approach

Recently [48], for the first time, the short nature of nucleon–nucleon correlations was accounted for based on the dependence of the SRC operator in spin and coordinate space. The new spin-dependent SRC correlation function is defined as

$$f_{SD}(r) = f(r) + g(r)\boldsymbol{\sigma_1}.\boldsymbol{\sigma_2}. \tag{16}$$

The transition operators for $0\nu\beta\beta$ decay incorporating spin-dependent SRCs are written as

$$\widetilde{O}^{\alpha}_{12} = f_{SD}(r)O^{\alpha}_{12}f_{SD}(r). \tag{17}$$

Using the relation $(\boldsymbol{\sigma_1}.\boldsymbol{\sigma_2})^2 = (3 - 2(\boldsymbol{\sigma_1}.\boldsymbol{\sigma_2}))$, the new Fermi operator of $0\nu\beta\beta$ decay is written as

$$\widetilde{O}^{F}_{12} = [f(r)^2 + 3g(r)^2]H_F(r) + (\boldsymbol{\sigma_1}.\boldsymbol{\sigma_2})2g(r)[f(r) - g(r)] * H_F(r) \tag{18}$$

and the Gamow–Teller operator of $0\nu\beta\beta$ decay is written as

$$\widetilde{O}^{GT}_{12} = [f(r)^2 - 4g(r)f(r) + 7g(r)^2]H_{GT}(r)(\boldsymbol{\sigma_1}.\boldsymbol{\sigma_2}) + 6g(r)[f(r) - g(r)]H_{GT}(r) \tag{19}$$

The functions $f(r)$ and $g(r)$ are defined as [48,50,51]

$$f(r) = a_1 - b_1e^{-c_1r^2} + d_1e^{-e_1(r-f_1)^2}, \tag{20}$$

$$g(r) = a_2e^{-b_2r^2}(1 + c_2r + d_2r^2). \tag{21}$$

The different parameters of $f(r)$ and $g(r)$ are presented in Table 2. These parameters are good for full fp and other configuration spaces. The authors of [48] may have considered only the $0f_{7/2}$ orbital as they wanted only to acquire initial insights through the pure shell model. Explicit details of using this SRC approach can be found in Ref. [50]. The derivation of the above formalism can be found in Refs. [50,51].

Table 2. Parameters of $f(r)$ and $g(r)$ for the spin-dependent SRCs.

Parameters for $f(r)$	Value	Parameters for $g(r)$	Value
a_1	1.00	a_2	0.04
b_1	0.92	b_2	1.39
c_1	2.56	c_2	2.92
d_1	0.33	d_2	−5.97
e_1	0.57		
f_1	−0.94		

In addition to the above, the authors of [52,53] have recently proposed another method, namely, the Unitary Correlation Operator Method [45–47], to estimate the effects of SRCs, which leads to a much smoother correction [44]. In the present study, we only focus on using a standard Jastrow-type approach and a spin-dependent approach to estimate

the effects of SRCs. Detailed descriptions of incorporating the SRC effects in different approaches can be found in Refs. [43,44].

It is worthwhile to mention that in a recent work [54], the short-range (SR) matrix element, a leading-order factor in light neutrino-exchange $0\nu\beta\beta$ decay, as established in a previous notable study [55], was meticulously computed. This calculation employed the generalized contact formalism (GCF) in conjunction with the shell model. The resulting total NME is composed of a long-range term, denoted as $M_L^{0\nu} = M_{GT} + M_F + M_T$, and a short-range term, $M_S^{0\nu}$. The investigation revealed a substantial contribution of the SR term to the total NME. Specifically, for nuclei with A = 48, $M_S^{0\nu}$ accounted for approximately 35–60% of $M_L^{0\nu}$. Moreover, it was observed that the SR term amplifies the total NME by 25–40% in heavier nuclei, indicating a significant impact on the half-life of $0\nu\beta\beta$ decay, while an intriguing avenue of inquiry lies in assessing how spin-dependent SRC effects might influence the SR matrix element, it should be noted that this current manuscript does not delve into that particular investigation, as it falls outside the scope of the present study. For those interested in a more comprehensive understanding of SR matrix elements, detailed information can be found in Refs. [54–56].

4. The Closure Method of NME Calculation for $0\nu\beta\beta$ Decay through the $(n-2)$ Channel

Now we discuss, including all the effects, how NMEs are calculated in the nuclear shell model. First, there are two approaches, nonclosure and closure. The nonclosure approach [24,36,37] considers the effects of excitation energies of a large number of intermediate states of the true virtual nucleus (^{48}Sc in the present case) explicitly through the denominator of Equation (7). In closure approximation [23], one approximates the term $E_k - (E_i + E_f)/2$ in the denominator of the neutrino potential of Equation (7) with a constant closure energy ($\langle E \rangle$) value such that

$$[E_k - (E_i + E_f)/2] \rightarrow \langle E \rangle. \tag{22}$$

Closure approximation avoids the complexity of calculating a large number of intermediate states, which can be computationally challenging for nuclear shell models for higher mass isotopes. The difficult part of closure approximation is picking the correct closure energy, which has no definite method yet and can greatly influence the accuracy of the calculated NMEs. Recently, there have been many studies of the nonclosure approach for $0\nu\beta\beta$ decay of ^{48}Ca [24,36,37], which predicted that $\langle E \rangle$ = 0.5 MeV is an optimal value of closure energy that gives values of the NMEs in the closure method very close to those in the nonclosure method. Hence, we use the closure method of NME calculation with a closure energy value $\langle E \rangle$ = 0.5 MeV.

Based on the closure approach, the M_{GT}, M_F, and M_T matrix elements of the scalar two-body transition operator O_{12}^{α} of $0\nu\beta\beta$ can be expressed as the sum over the product of the two-body transition density (TBTD) and anti-symmetric two-body matrix elements ($\langle k_1', k_2', JT|O_{12}^{\alpha}|k_1, k_2, JT\rangle_A$). For the first, we write the partial NME as a function of the coupled spin-parity (J^{π}) of protons and neutrons and a number of intermediate states (N_m) of the TBTD calculations as [25]

$$M_{\alpha}(J^{\pi}, N_m) = \sum_{k_1' \leq k_2', k_1 \leq k_2} \text{TBTD}(f, m, i, J^{\pi}) \langle k_1', k_2', J^{\pi}T|O_{12}^{\alpha}|k_1, k_2, J^{\pi}T\rangle_A, \tag{23}$$

such that the final required Fermi, GT, and tensor-type NME of Equation (5) can be written as

$$M_{\alpha} = \sum_{J, N_m \leqslant N_c} M_{\alpha}(J^{\pi}, N_m), \tag{24}$$

where, $\alpha = (F, GT, T)$, J^π is the coupled spin-parity of two decaying neutrons or two final created protons, A denotes that the two-body matrix elements are obtained using anti-symmetric two-nucleon wave functions, k stands for the set of spherical quantum numbers $(n; l; j)$, N_c is cutoff on number of states of intermediate nucleus (^{46}Ca in the present case) for TBTD calculations. In our case, $|i\rangle$ is 0^+ g.s. of the parent nucleus ^{48}Ca, $|f\rangle$ is the 0^+ g.s. of the granddaughter nucleus ^{48}Ti, and k has the spherical quantum numbers for $0f_{7/2}$, $0f_{5/2}$, $1p_{3/2}$, and $1p_{1/2}$ orbitals. The TBTD can be expressed as [25]

$$\mathrm{TBTD}(f, m, i, J) = \langle f||[A^+(k_1', k_2', J) \otimes \tilde{A}(k_1, k_2, J)]^{(0)}||i\rangle, \tag{25}$$

where,

$$A^+(k_1', k_2', J) = \frac{[a^+(k_1') \otimes a^+(k_2')]^J_M}{\sqrt{1 + \delta_{k_1' k_2'}}}, \tag{26}$$

and

$$\tilde{A}(k_1, k_2, J) = (-1)^{J-M} A^+(k_1, k_2, J, -M) \tag{27}$$

are the two-particle creation and annihilation operators of rank J, respectively.

To evaluate TBTD, one needs a large number of two-nucleon transfer amplitudes (TNAs). The TNAs are calculated with a large set of intermediate states $|m\rangle$ of the (n-2) nucleon system (^{46}Ca in the present study), where n is the number of nucleons for the parent nucleus. The TBTD in terms of TNAs is expressed as [25]

$$\mathrm{TBTD}(f, m, i, J) = \sum_m \mathrm{TNA}(f, m, k_1', k_2', J_m)\mathrm{TNA}(i, m, k_1, k_2, J_m), \tag{28}$$

where the TNAs are given by

$$\mathrm{TNA}(f, m, k_1', k_2', J_m) = \frac{\langle f||A^+(k_1', k_2', J)||m\rangle}{\sqrt{2J_0 + 1}}. \tag{29}$$

Here, J_m is the spin of the allowed states of ^{46}Ca, J_0 is spin of $|i\rangle$ and $|f\rangle$, and $J_m = J$ when $J_0 = 0$ [25].

5. Results and Discussion

The TNAs are evaluated utilizing the nuclear shell model. For this purpose, we employ the KSHELL code [57], which facilitates the computation of essential wave functions and energies concerning the initial, intermediate, and final nuclei involved in the $0\nu\beta\beta$ decay process of ^{48}Ca. Subsequently, these calculated wave functions are harnessed to determine the TNAs, a pivotal component within the expression of NMEs for the $0\nu\beta\beta$ decay.

For these calculations, we utilize the shell model Hamiltonian GXPF1A [58], tailored for the fp model space, serving as a foundational input for our computations.

The fp model space comprises the $f_{7/2}$, $p_{3/2}$, $f_{5/2}$, and $p_{1/2}$ orbitals. The computation of the two-body matrix element (TBME) components within the NMEs is executed using a proprietary code developed by us. The outcomes of distinct NME types, computed through the shell model approach with the Jastrow methodology employing various SRC parameterizations, and spin-dependent SRCs are presented in Table 3.

Table 3. NMEs for $0\nu\beta\beta$ decay (the light neutrino-exchange mechanism) of ^{48}Ca calculated with nuclear shell model for spin-dependent SRCs and Jastrow-type SRCs with different parameterizations. Calculations are conducted within the closure approximation in the $(n-2)$ channel, employing the GXPF1A effective shell model Hamiltonian.

NME Type	SRC Type	NME Value
M_F	None	-0.215
M_F	Miller–Spencer	-0.144
M_F	CD-Bonn	-0.232
M_F	AV18	-0.213
M_F	Spin-Dependent SRCs	-0.190
M_{GT}	None	0.774
M_{GT}	Miller–Spencer	0.540
M_{GT}	CD-Bonn	0.806
M_{GT}	AV18	0.740
M_{GT}	Spin-Dependent SRCs	0.674
$M^{0\nu}$	None	0.873
$M^{0\nu}$	Miller–Spencer	0.629
$M^{0\nu}$	CD-Bonn	0.950
$M^{0\nu}$	AV18	0.872
$M^{0\nu}$	Spin-Dependent SRCs	0.792

It is important to note that the presentation of tensor-type NMEs is omitted from Table 3 due to the lack of a solvable expression for the TBMEs inclusive of the spin-dependent SRC function specified in Equation (16). This is not a critical concern as the Gamow–Teller (GT) and Fermi-type NMEs overwhelmingly dominate over tensor-type NMEs. Therefore, in Table 3, the calculation of total NMEs solely considers the Fermi and GT-type contributions.

The NMEs corresponding to the application of spin-dependent SRCs are approximately 10% diminished in comparison to those calculated with AV18-type NMEs, as well as SRC-none scenarios, across Fermi, Gamow–Teller (GT), and total NMEs. In contrast, when gauged against CD-Bonn-type, the NMEs with spin-dependent SRCs experience a more pronounced reduction, approximately 20%, across Fermi, GT, and total NMEs.

Remarkably, among the various SRC parameterizations, the Miller–Spencer-type NMEs manifest the most pronounced impact of SRC. Notably, NMEs with spin-dependent SRC showcase an expansion of approximately 20% relative to Miller–Spencer type NMEs, encompassing the realms of Fermi, GT, and total NMEs.

As mentioned above, the main findings of Ref. [48] is that accounting for spin-dependent SRsC leads to an approximate 20% reduction in NME values when compared to the no-SRC scenario within the pure shell model framework. In our analysis, we observe a comparable 10% decrease in NME values under the same conditions relative to the no-SRC case, but in the interacting shell model. These differences may be attributed to our consideration of the entire fp model space, encompassing $0f_{7/2}$, $0f_{5/2}$, $1p_{3/2}$, and $1p_{1/2}$ orbitals in contrast to the approach in Ref. [48], which employed a simplified shell model with a single active orbital, $0f_{7/2}$.

5.1. Dependence of NMEs on Coupled Spin-Parity (J^π) of Two Decaying Neutrons and Two Created Protons

Next, we examine the comparison of the contributions from different coupled spin-parities in the NMEs for CD-Bonn-type NMEs and spin-dependent SRCs. To do this, we decompose NMEs in terms of partial nuclear matrix elements of coupled spin-parity (J^π) of two decaying neutrons or two created protons as

$$M_\alpha(J^\pi) = \sum_{N_m \leq N_c} M_\alpha(J^\pi, N_m), \tag{30}$$

where one can define $M^{0\nu}_{\alpha}(J^{\pi})$ using Equation (23). It should be noted that j^{π} in the above equation also represents the spin-parity of the states of the intermediate nucleus ^{46}Ca.

The contributions of NMEs through different J^{π} are shown in Figure 1. We observe that for all types of NMEs, the most dominant contributions come from the 0^{+} and 2^{+} states. Additionally, the contribution from the 0^{+} and 2^{+} states have opposite signs, leading to a reduction in the total NMEs. There are also small contributions from the 4^{+} and 6^{+} states, with almost negligible contributions from odd-J^{π} states. This is due to the pairing effect, which is responsible for the dominance of even-J^{π} contributions [25]. Note that spin-dependent SRCs are smaller in magnitude than CD-Bonn-type SRC parameterizations. However, the overall pattern of dependence on J^{π} is very similar for both SRCs.

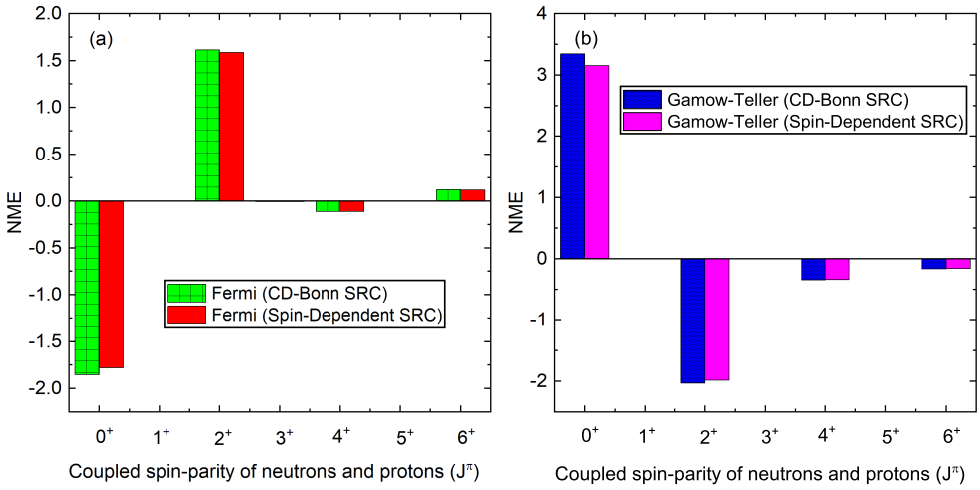

Figure 1. (Color online) Contribution of various coupled spin-parity states (J^{π}) of two initial neutrons or two final created protons for (**a**) Fermi-type and (**b**) Gamow–Teller-type NMEs. The illustrated NMEs pertain to the light neutrino-exchange mechanism in the context of $0\nu\beta\beta$ decay of ^{48}Ca. Calculations have been carried out utilizing the nuclear shell model, considering both CD-Bonn and spin-dependent SRCs.

5.2. Variation in NMEs for $0\nu\beta\beta$ with the Cutoff Number of States (N_c) of ^{46}Ca

To assess the impact of the number of states on the calculated NMEs, we examine the dependence of the NMEs on the cutoff number of states (N_c) for each allowed J^{π}_{m} of ^{46}Ca, which acts as an intermediate nucleus for TNA calculations. Shell model code packages like KSHELL do not provide options for setting a cutoff for the excitation energy, which may be more relevant, but they do provide options to set a cutoff for the number of states for each spin-parity of the intermediate states of ^{46}Ca. Hence, we consider a certain number of intermediate states for each spin-parity of ^{46}Ca with a cutoff according to the computational power available for the calculations. We express the NMEs as a function of N_c in the closure method as

$$M_{\alpha} = \sum_{J, N_m \leqslant N_c} M_{\alpha}(J^{\pi}, N_m) \tag{31}$$

where $M_{\alpha}(J^{\pi}, N_m)$ is the same as that defined in Equation (23).

The dependence of the different types of NMEs on N_c is shown in Figure 2. We compare the results for CD-Bonn-type SRC parameterization with spin-dependent SRCs. We find that the first few low-lying states contribute constructively and destructively, but after $N_c = 30$, the different types of NMEs reach a stable value. For larger N_c, the NMEs become mostly constant. To obtain NMEs with negligible uncertainty, we were able to consider $N_c = 100$ for each allowed J^{π}_{m} of ^{46}Ca. We note that a similar dependence of NMEs on N_c is seen for other SRC parameterizations. The overall pattern of dependence of NMEs

on N_c for spin-dependent SRCs and CD-Bonn-type SRCs is similar, but spin-dependent SRC NMEs are much smaller in magnitude compared to NMEs for CD-Bonn-type SRCs.

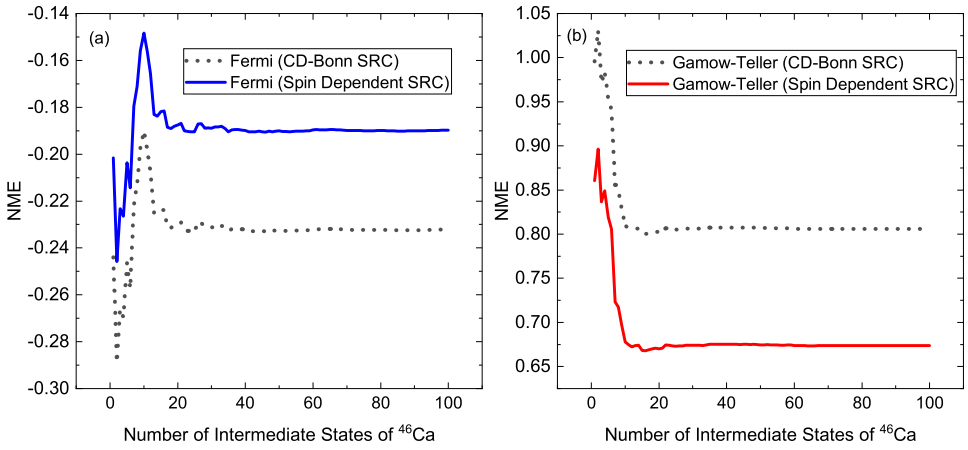

Figure 2. (Color online) The graph illustrates the variation in (**a**) Fermi and (**b**) Gamow-Teller NMEs for the $0\nu\beta\beta$ (the light neutrino-exchange mechanism) of ^{48}Ca with the cutoff number of states (N_c) of the intermediate nucleus ^{46}Ca (for TNA calculation). The NMEs are calculated using the GXPF1A Hamiltonian for CD-Bonn-type and spin-dependent SRCs.

5.3. Neutrino Momentum (q) and Radial (r) Distribution of NMEs

We have also examined the neutrino momentum transfer (q) distribution of NMEs. One can define q dependent distribution ($C_\alpha(q)$) such that the NME defined in Equation (5) can be written as [59]

$$M_\alpha = \int_0^\infty C_\alpha(q)dq. \tag{32}$$

The distribution of different $C_\alpha(q)$ is shown in Figure 3. Here, NMEs are compared for CD-Bonn-type SRC parameterization and spin-dependent SRCs. It is found that most of the contributions of the NMEs come from q below 500 MeV. The peak contributions come from q around 10 MeV and 180 MeV with a peak value around 0.003 MeV^{-1} for GT-type NMEs with CD-Bonn-type SRCs and a peak value around 0.0027 MeV^{-1} for GT-type NMEs with spin-dependent SRCs. The peak value for Fermi-type NMEs is around -0.001 MeV^{-1} for both CD-Bonn-type and spin-dependent SRCs. The overall pattern of the dependence of NMEs for both CD-Bonn-type and spin-dependent SRCs is similar.

The radial distribution of NMEs is also explored. One can write the radial-dependent NME distribution ($C_\alpha(r)$) [42,59,60] such that

$$M_\alpha = \int_0^\infty C_\alpha(r)dr. \tag{33}$$

The distribution of different $C_\alpha(r)$ is shown in Figure 4. Here, NMEs are calculated using the closure method for CD-Bonn-type and spin-dependent SRCs with $\langle E \rangle$ = 0.5 MeV. It is found that most of the contribution comes from r less than 4 fm. The NMEs peak around 1 fm for both CD-Bonn-type and spin-dependent SRCs. The maximum value for $C_\alpha(r)$ is near 1.2 fm^{-1} For GT-type and around -0.5 fm^{-1} for Fermi-type NMEs for both CD-Bonn-type and spin-dependent SRCs. Here also, the overall pattern of variation for CD-Bonn-type and spin-dependent SRCs is similar, but they differ slightly in magnitude.

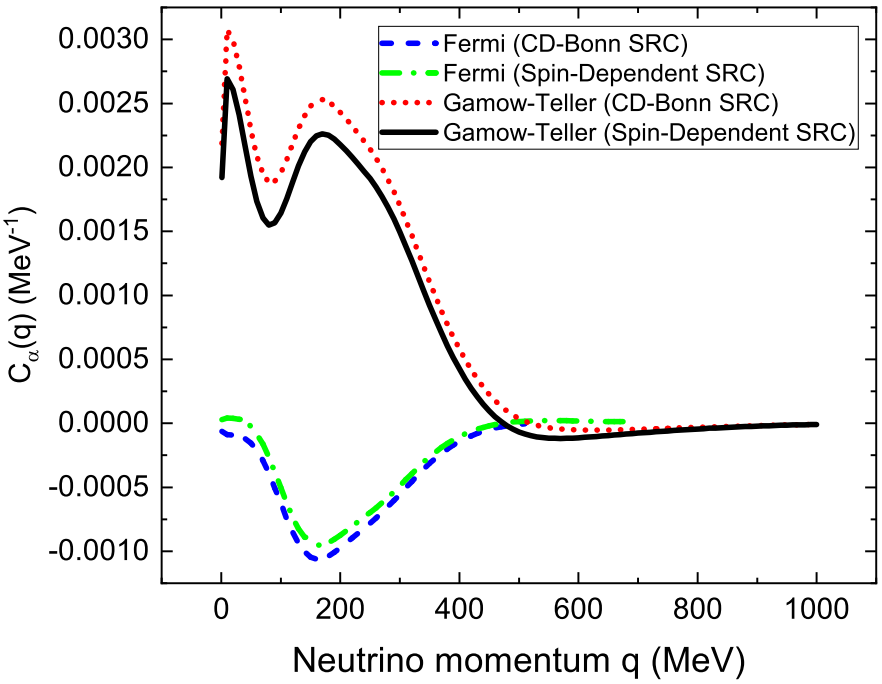

Figure 3. (Color online) Distribution of NMEs ($C_\alpha(q)$) with neutrino momentum (q) transfer. The NMEs are computed employing the closure method, considering both CD-Bonn-type SRC parameterization and spin-dependent SRCs. These calculations are executed utilizing the GXPF1A Hamiltonian with closure energy $\langle E \rangle$ = 0.5 MeV.

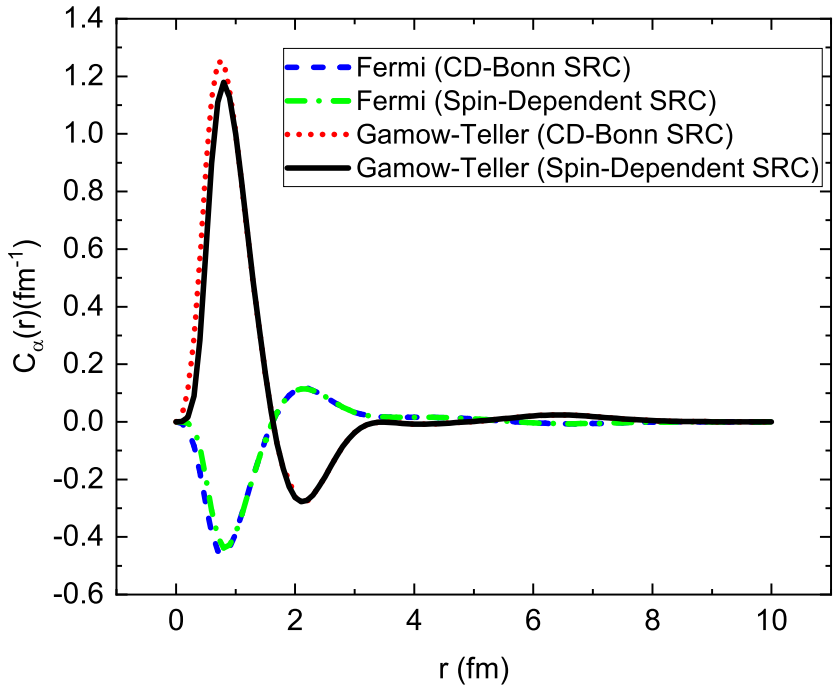

Figure 4. (Color online) Radial distribution of NMEs ($C_\alpha(r)$) with inter-nucleon distance (r). The NMEs have been computed utilizing the closure method, considering both CD-Bonn-type SRC parameterization and spin-dependent SRCs. These calculations are performed using the GXPF1A Hamiltonian with a closure energy $\langle E \rangle$ = 0.5 MeV.

5.4. Variation in NMEs with Closure Energy

Finally, we also show the variation in different types of total NMEs with closure energy $\langle E \rangle$ in Figure 5. The NMEs shown here are the total NMEs in different parameterizations of

the Jastrow-type approach and spin-dependent approach. In total NMEs, the Fermi- and GT-type NMEs are only considered, and tensor-type NME is not included for the reason mentioned above. In changing $\langle E \rangle$ = 0 to 15 MeV, there are about 10–15% decrements of total NMEs in the closure method. Other than varying in magnitude, the spin-dependent SRCs vary very similarly to other SRC parameterizations of the Jastrow-type approach.

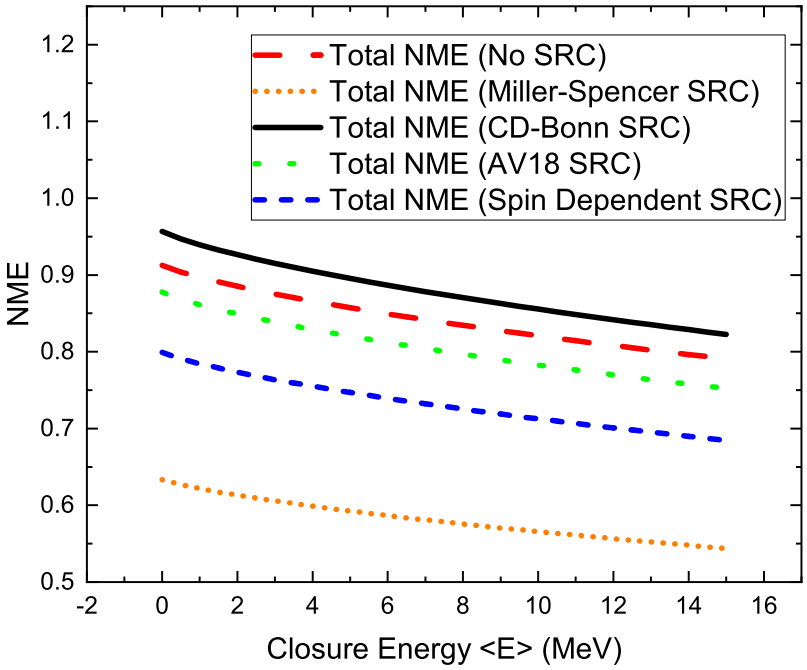

Figure 5. (Color online) Variation in total NMEs pertaining to the $0\nu\beta\beta$ decay via the light neutrino-exchange mechanism in ^{48}Ca, in relation to the closure energy $\langle E \rangle$. These computations employ the GXPF1A Hamiltonian and adopt different SRC parameterizations through the closure method. It is worth noting that the calculation of total NMEs does not encompass the tensor-type NMEs.

6. Summary and Conclusions

In summary, our investigation has centered on comprehensively exploring the effects of spin-dependent SRCs on the NMEs associated with the light neutrino-exchange $0\nu\beta\beta$ decay of ^{48}Ca. This exploration was juxtaposed with the traditional Jastrow-type approach to SRCs, employing diverse parameterizations. All computations were performed within the framework of a nuclear shell model, incorporating the closure approximation and utilizing the GXPF1A Hamiltonian to encapsulate the complete fp model space. The nuclear wave functions were derived through shell model diagonalization, leveraging the KSHELL code. These derived wave functions formed the bedrock for evaluating a multitude of TNAs, integral to the formulation of the NMEs. The segment concerning TBMEs within the NMEs was computed through code developed by us.

Beyond the comparison of the NMEs of different types (Fermi, Gamow, and total) originating from spin-dependent SRCs and Jastrow-type SRCs, our analysis delved into the comparative dependencies of NMEs linked to attributes such as the coupled spin-parity of protons and neutrons, the number of intermediate states of TNA calculation, neutrino momentum, radial separation, and closure energy.

Our findings prominently highlight a discernible reduction in NMEs resulting from the application of spin-dependent SRCs, exhibiting, for instance, a 10–20% decrease in NMEs when contrasted with Jastrow-type SRCs with diverse parameterizations. This substantial variation may bear noticeable implications for half-life and neutrino mass considerations. At the same time, while exhibiting a different magnitude, the general pattern of variation in NMEs under the influence of spin-dependent SRCs still bears a resemblance to that observed with the Jastrow-type approach.

In our forthcoming research, our aim is to extend the influence of the spin-dependent SRC approach to encompass other candidates for $0\nu\beta\beta$ decay, exploring a spectrum of mechanisms and scenarios.

Author Contributions: Validation: S.S. and Y.I. Original Draft Preparation: S.S. and Y.I. Writing—Review and Editing: S.S. and Y.I. Both authors have made equal contributions throughout multiple phases of calculations and the formulation of the final manuscript. All authors have read and agreed to the published version of the manuscript.

Funding: S.S. is thankful to the Science and Engineering Research Board (SERB), Department of Science and Technology (DST), Government of India, for the award of the SERB-National Postdoctoral Fellowship under Grant No. PDF/2022/003729.

Data Availability Statement: No new data were created or analyzed in this study. Data sharing is not applicable to this article.

Acknowledgments: S.S. expresses profound gratitude to Rajdeep Chatterjee for the invaluable mentorship received throughout the tenure as a SERB-National Postdoctoral Fellow at the Indian Institute of Technology Roorkee. S.S. also acknowledges the National Supercomputing Mission (NSM) for providing computing resources of 'PARAM Ganga' at the Indian Institute of Technology Roorkee, which is implemented by C-DAC and supported by the Ministry of Electronics and Information Technology (MeitY) and Department of Science and Technology (DST), Government of India.

Conflicts of Interest: The authors declare no conflict of interest.

References

1. Agostini, M.; Benato, G.; Detwiler, J.A.; Menéndez, J.; Vissani, F. Toward the discovery of matter creation with neutrinoless $\beta\beta$ decay. *Rev. Mod. Phys.* **2023**, *95*, 025002. [CrossRef]
2. Dolinski, M.J.; Poon, A.W.P.; Rodejohann, W. Neutrinoless Double-Beta Decay: Status and Prospects. *Ann. Rev. Nucl. Part. Sci.* **2019**, *69*, 219–251. [CrossRef]
3. Vergados, J.D.; Ejiri, H.; Šimkovic, F. Neutrinoless double beta decay and neutrino mass. *Int. J. Mod. Phys. E* **2016**, *25*, 1630007. [CrossRef]
4. Engel, J.; Menéndez, J. Status and future of nuclear matrix elements for neutrinoless double-beta decay: A review. *Rep. Prog. Phys.* **2017**, *80*, 046301. [CrossRef]
5. Avignone, F.T.; Elliott, S.R.; Engel, J. Double beta decay, Majorana neutrinos, and neutrino mass. *Rev. Mod. Phys.* **2008**, *80*, 481–516. [CrossRef]
6. Furry, W.H. On Transition Probabilities in Double Beta-Disintegration. *Phys. Rev.* **1939**, *56*, 1184–1193. [CrossRef]
7. Vergados, J.D.; Ejiri, H.; Šimkovic, F. Theory of neutrinoless double-beta decay. *Rep. Prog. Phys.* **2012**, *75*, 106301. [CrossRef] [PubMed]
8. Majorana, E. Symmetric theory of electron and positron. *Il Nuovo Cimento (1924–1942)* **1937**, *14*, 171. [CrossRef]
9. Racah, G. Sulla simmetria tra particelle e antiparticelle. *Il Nuovo Cimento* **1937**, *14*, 322. [CrossRef]
10. Deppisch, F.F.; Hirsch, M.; Päs, H. Neutrinoless double-beta decay and physics beyond the standard model. *J. Phys. G Nucl. Part. Phys.* **2012**, *39*, 124007. [CrossRef]
11. Schechter, J.; Valle, J.W. Neutrinoless double-β decay in SU (2)$\times$ U (1) theories. *Phys. Rev. D* **1982**, *25*, 2951. [CrossRef]
12. Rodejohann, W. Neutrino-less double beta decay and particle physics. *Int. J. Mod. Phys. E* **2011**, *20*, 1833–1930. [CrossRef]
13. Aker, M.; Beglarian, A.; Behrens, J.; Berlev, A.; Besserer, U.; Bieringer, B.; Block, F.; Bobien, S.; Bottcher, M.; Bornschein, B.; et al. Direct neutrino-mass measurement with sub-electronvolt sensitivity. *Nat. Phys.* **2022**, *18*, 160–166. [CrossRef]
14. KamLAND-Zen Collaboration. Search for the Majorana Nature of Neutrinos in the Inverted Mass Ordering Region with KamLAND-Zen. *Phys. Rev. Lett.* **2023**, *130*, 051801. [CrossRef]
15. Tomoda, T. Double beta decay. *Rep. Prog. Phys.* **1991**, *54*, 53. [CrossRef]
16. Rodin, V.; Faessler, A.; Šimkovic, F.; Vogel, P. Assessment of uncertainties in QRPA $0\nu\beta\beta$-decay nuclear matrix elements. *Nucl. Phys. A* **2006**, *766*, 107–131. [CrossRef]
17. Šimkovic, F.; Pantis, G.; Vergados, J.D.; Faessler, A. Additional nucleon current contributions to neutrinoless double β decay. *Phys. Rev. C* **1999**, *60*, 055502. [CrossRef]
18. Mohapatra, R.N.; Senjanović, G. Neutrino Mass and Spontaneous Parity Nonconservation. *Phys. Rev. Lett.* **1980**, *44*, 912–915. [CrossRef]
19. Mohapatra, R.N.; Vergados, J.D. New Contribution to Neutrinoless Double Beta Decay in Gauge Models. *Phys. Rev. Lett.* **1981**, *47*, 1713–1716. [CrossRef]
20. Mohapatra, R.N. New contributions to neutrinoless double-beta decay in supersymmetric theories. *Phys. Rev. D* **1986**, *34*, 3457–3461. [CrossRef]

21. Vergados, J. Neutrinoless double β-decay without Majorana neutrinos in supersymmetric theories. *Phys. Lett. B* **1987**, *184*, 55–62. [CrossRef]
22. Caurier, E.; Menéndez, J.; Nowacki, F.; Poves, A. Influence of Pairing on the Nuclear Matrix Elements of the Neutrinoless $\beta\beta$ Decays. *Phys. Rev. Lett.* **2008**, *100*, 052503. [CrossRef]
23. Horoi, M.; Stoica, S. Shell model analysis of the neutrinoless double-β decay of ^{48}Ca. *Phys. Rev. C* **2010**, *81*, 024321. [CrossRef]
24. Sen'kov, R.A.; Horoi, M. Neutrinoless double-β decay of ^{48}Ca in the shell model: Closure versus nonclosure approximation. *Phys. Rev. C* **2013**, *88*, 064312. [CrossRef]
25. Brown, B.A.; Horoi, M.; Sen'kov, R.A. Nuclear Structure Aspects of Neutrinoless Double-β Decay. *Phys. Rev. Lett.* **2014**, *113*, 262501. [CrossRef]
26. Iwata, Y.; Shimizu, N.; Otsuka, T.; Utsuno, Y.; Menéndez, J.; Honma, M.; Abe, T. Large-Scale Shell-Model Analysis of the Neutrinoless $\beta\beta$ Decay of ^{48}Ca. *Phys. Rev. Lett.* **2016**, *116*, 112502. [CrossRef] [PubMed]
27. Barea, J.; Iachello, F. Neutrinoless double-β decay in the microscopic interacting boson model. *Phys. Rev. C* **2009**, *79*, 044301. [CrossRef]
28. Barea, J.; Kotila, J.; Iachello, F. Limits on Neutrino Masses from Neutrinoless Double-β Decay. *Phys. Rev. Lett.* **2012**, *109*, 042501. [CrossRef]
29. Rodríguez, T.R.; Martínez-Pinedo, G. Energy Density Functional Study of Nuclear Matrix Elements for Neutrinoless $\beta\beta$ Decay. *Phys. Rev. Lett.* **2010**, *105*, 252503. [CrossRef]
30. Song, L.S.; Yao, J.M.; Ring, P.; Meng, J. Relativistic description of nuclear matrix elements in neutrinoless double-β decay. *Phys. Rev. C* **2014**, *90*, 054309. [CrossRef]
31. Yao, J.M.; Song, L.S.; Hagino, K.; Ring, P.; Meng, J. Systematic study of nuclear matrix elements in neutrinoless double-β decay with a beyond-mean-field covariant density functional theory. *Phys. Rev. C* **2015**, *91*, 024316. [CrossRef]
32. Rath, P.K.; Chandra, R.; Chaturvedi, K.; Raina, P.K.; Hirsch, J.G. Uncertainties in nuclear transition matrix elements for neutrinoless $\beta\beta$ decay within the projected-Hartree-Fock-Bogoliubov model. *Phys. Rev. C* **2010**, *82*, 064310. [CrossRef]
33. Pastore, S.; Carlson, J.; Cirigliano, V.; Dekens, W.; Mereghetti, E.; Wiringa, R.B. Neutrinoless double-β decay matrix elements in light nuclei. *Phys. Rev. C* **2018**, *97*, 014606. [CrossRef]
34. Wang, X.B.; Hayes, A.; Carlson, J.; Dong, G.; Mereghetti, E.; Pastore, S.; Wiringa, R.B. Comparison between variational Monte Carlo and shell model calculations of neutrinoless double beta decay matrix elements in light nuclei. *Phys. Lett. B* **2019**, *798*, 134974. [CrossRef]
35. Cirigliano, V.; Dekens, W.; de Vries, J.; Graesser, M.L.; Mereghetti, E.; Pastore, S.; Piarulli, M.; van Kolck, U.; Wiringa, R.B. Renormalized approach to neutrinoless double-β decay. *Phys. Rev. C* **2019**, *100*, 055504. [CrossRef]
36. Sarkar, S.; Iwata, Y.; Raina, P.K. Nuclear matrix elements for the λ mechanism of $0\nu\beta\beta$ decay of ^{48}Ca in the nuclear shell-model: Closure versus nonclosure approach. *Phys. Rev. C* **2020**, *102*, 034317. [CrossRef]
37. Sarkar, S.; Kumar, P.; Jha, K.; Raina, P.K. Sensitivity of nuclear matrix elements of $0\nu\beta\beta$ of ^{48}Ca to different components of the two-nucleon interaction. *Phys. Rev. C* **2020**, *101*, 014307. [CrossRef]
38. Ahmed, F.; Horoi, M. Interference effects for $0\nu\beta\beta$ decay in the left-right symmetric model. *Phys. Rev. C* **2020**, *101*, 035504. [CrossRef]
39. Horoi, M.; Neacsu, A. Shell model study of using an effective field theory for disentangling several contributions to neutrinoless double-β decay. *Phys. Rev. C* **2018**, *98*, 035502. [CrossRef]
40. Horoi, M. Shell model analysis of competing contributions to the double-β decay of ^{48}Ca. *Phys. Rev. C* **2013**, *87*, 014320. [CrossRef]
41. Neacsu, A.; Stoica, S.; Horoi, M. Fast, efficient calculations of the two-body matrix elements of the transition operators for neutrinoless double-β decay. *Phys. Rev. C* **2012**, *86*, 067304. [CrossRef]
42. Menendez, J.; Poves, A.; Caurier, E.; Nowacki, F. Disassembling the Nuclear Matrix Elements of the Neutrinoless beta beta Decay. *Nucl. Phys. A* **2009**, *818*, 139–151. [CrossRef]
43. Šimkovic, F.; Faessler, A.; Müther, H.; Rodin, V.; Stauf, M. $0\nu\beta\beta$-decay nuclear matrix elements with self-consistent short-range correlations. *Phys. Rev. C* **2009**, *79*, 055501. [CrossRef]
44. Vogel, P. Nuclear structure and double beta decay. *J. Phys. G Nucl. Part. Phys.* **2012**, *39*, 124002. [CrossRef]
45. Feldmeier, H.; Neff, T.; Roth, R.; Schnack, J. A unitary correlation operator method. *Nucl. Phys. A* **1998**, *632*, 61–95. [CrossRef]
46. Neff, T.; Feldmeier, H. Tensor correlations in the unitary correlation operator method. *Nucl. Phys. A* **2003**, *713*, 311–371. [CrossRef]
47. Roth, R.; Neff, T.; Hergert, H.; Feldmeier, H. Nuclear structure based on correlated realistic nucleon–nucleon potentials. *Nucl. Phys. A* **2004**, *745*, 3–33. [CrossRef]
48. Benhar, O.; Biondi, R.; Speranza, E. Short-range correlation effects on the nuclear matrix element of neutrinoless double-β decay. *Phys. Rev. C* **2014**, *90*, 065504. [CrossRef]
49. Kotila, J.; Iachello, F. Phase-space factors for double-β decay. *Phys. Rev. C* **2012**, *85*, 034316. [CrossRef]
50. Speranza, E. Correlation Effects on the Nuclear Matrix Element of Neutrinoless Double β-Decay. Master's Thesis, Sapienza University of Rome, Roma, Italy, December 2011.
51. Valli, M. Shear Viscosity of Neutron Matter from Realistic Nucleon-Nucleon Interactions. Ph.D. Thesis, Sapienza University of Rome, Roma, Italy, 2007.
52. Kortelainen, M.; Civitarese, O.; Suhonen, J.; Toivanen, J. Short-range correlations and neutrinoless double beta decay. *Phys. Lett. B* **2007**, *647*, 128–132. [CrossRef]

53. Kortelainen, M.; Suhonen, J. Improved short-range correlations and $0\nu\beta\beta$ nuclear matrix elements of ^{76}Ge and ^{82}Se. *Phys. Rev. C* **2007**, *75*, 051303. [CrossRef]
54. Weiss, R.; Soriano, P.; Lovato, A.; Menendez, J.; Wiringa, R.B. Neutrinoless double-β decay: Combining quantum Monte Carlo and the nuclear shell model with the generalized contact formalism. *Phys. Rev. C* **2022**, *106*, 065501. [CrossRef]
55. Cirigliano, V.; Dekens, W.; de Vries, J.; Graesser, M.L.; Mereghetti, E.; Pastore, S.; van Kolck, U. New Leading Contribution to Neutrinoless Double-β Decay. *Phys. Rev. Lett.* **2018**, *120*, 202001. [CrossRef] [PubMed]
56. Jokiniemi, L.; Soriano, P.; Menéndez, J. Impact of the leading-order short-range nuclear matrix element on the neutrinoless double-beta decay of medium-mass and heavy nuclei. *Phys. Lett. B* **2021**, *823*, 136720. [CrossRef]
57. Shimizu, N.; Mizusaki, T.; Utsuno, Y.; Tsunoda, Y. Thick-Restart Block Lanczos Method for Large-Scale Shell-Model Calculations. *Comput. Phys. Commun.* **2019**, *244*, 372–384. [CrossRef]
58. Caurier, E.; Nowacki, F.; Poves, A.; Sieja, K. Collectivity in the light xenon isotopes: A shell model study. *Phys. Rev. C* **2010**, *82*, 064304. [CrossRef]
59. Menéndez, J. Neutrinoless $\beta\beta$ decay mediated by the exchange of light and heavy neutrinos: The role of nuclear structure correlations. *J. Phys. G Nucl. Part. Phys.* **2017**, *45*, 014003. [CrossRef]
60. Šimkovic, F.; Faessler, A.; Rodin, V.; Vogel, P.; Engel, J. Anatomy of the $0\nu\beta\beta$ nuclear matrix elements. *Phys. Rev. C* **2008**, *77*, 045503. [CrossRef]